Phase diagrams of a lattice-gas model for micellar binary solutions

1996 J. Phys.: Condens. Matter 8 3347

(http://iopscience.iop.org/0953-8984/8/19/010)

J. Phys.: Condens. Matter **8** (1996) 3347–3361. Printed in the UK

Phase diagrams of a lattice-gas model for micellar binary solutions

A Benyoussef†, L Laanait‡, N Masaif†§ and N Moussa†

† Laboratoire de Magnetisme et Physique des Hautes Energies, Faculté des Sciences, BP 1014, Rabat, Morocco

‡ Ecole Normale Supérieure, BP 5118, Rabat, Morocco

§ LPT Department de Physique, Faculté des Sciences et Techniques, BP 577, Settat, Morocco

Received 26 July 1995, in final form 17 October 1995

Abstract. Using the mean-field approximation, we study the phase diagrams of the micellar binary solutions in the presence of a chemical potential of the amphiphiles (h) and the attraction interaction intermicellar parameter (J) for different values of competing interactions (K_0 and K_1).

1. Introduction

One of the most fascinating and challenging problems of contemporary experimental and theoretical physics has been that of achieving an understanding of the characteristic of phase diagrams of amphiphic systems.

Recently, several models of binary mixtures of amphiphile (a molecule of both hydrophilic and hydrophobic parts) and water have been proposed in order to reproduce the phases observed experimentally [1–6].

In general, the amphiphile molecules in the water–amphiphile mixtures try to arrange themselves as to only expose their polar head groups to the water molecules. In particular, when the amphiphile is wholly immersed in water, the molecules again try to reduce the area of contact with water in order to form aggregates (rods, spheres, lammellar, ...). Precisely, when a hydrocarbon is in contact with water, the network of hydrogen bonds between water molecules reconstructs itself to avoid the region occupied by hydrocarbon. This constraint on the local structure of water decreases the entropy near the hydrocarbon, and it results in an increase of the free energy of the system [7].

For amphiphilic systems, the aggregation of molecules of the binary solution induces multiple equilibrium processes controlled by intermolecular and interaggregate forces [8]. Micellar aggregates appear in various shapes and sizes, depending on the amphiphiles, the concentration and other thermodynamic parameters. This suggests a classification of the aggregates into three general categories as follows: (i) globular aggregates, where a spherical micelle is a prototype of this class; (ii) rodlike aggregates, where a cylindrical micelle is the typical example of this class; (iii) bilayers, where a disclike aggregate is an example of this class. The choice among all the possible shapes is determined by interactions between the hydrophilic headgroups and geometric packing constraints on the hydrophobic tails, but the transition from one shape to another may be obtained by changing either the temperature or the concentration or by adding a third component.

0953-8984/96/193347+15$19.50

Gelbart *et al* [6] have provided an introduction to micellization phenomena in aqueous surfactant solutions. The discussion presented by these authors has been restricted to the case of dilute solutions where interaction between micellar aggregates can be neglected.

With increasing amphiphile concentration a variety of lyotropic phases are found [14, 8, 10, 11]. The phase diagram for the system of water and $C_{12}E_8$ (i.e. $C_{12}H_{25}(OCH_2CH_2)_8OH$) and for water and $C_{12}E_5$ has been produced respectively by Degiorgio *et al* [13] and Strey *et al* [12] representing such phenomena.

At low temperatures, Gompper and Schick [4] and Matsen and Sullivan [3] have exhibited within mean-field theory a two-phase coexistence between homogeneous water-rich and amphiphile-rich phases, but at higher temperatures there is a single disordered phase. The phase diagram established in [4] resembles that of the system of $C_{12}E_8$ and water [8] for which scattering experiments have been carried out [13], that is, the model employed in [4] is a generalization of one considered by Halley and Kolan [2].

Concerning the microscopic approach, Shnidman and Zia [15] recently proposed a lattice-gas model, based on constructing a coarse-grained representation of different types of aggregate occurring in micellar binary solutions (MBS's) in terms of Ising variables. One introduces on a lattice site (i, j) the Ising variable satisfying $s_{i,j} = +1$ for a micellar section and $s_{i,j} = -1$ describes a region, of comparable size, predominantly occupied by a solvent.

A single $+1$ spin completely surrounded by -1 spins is identified with a globular micelle, and a linear chain of $+1$ spins surrounded by -1 spins corresponds to a rodlike micelle. Finally, a spin $+1$ at the end of a chain of $+1$ spins surrounded by -1 spins is called an end cap [15].

In this paper we propose a description, within the mean-field approximation, of phase diagrams of the MBSs in two dimensions in the space of the parameters T (temperature) and h (chemical potential of the amphiphiles) for different fixed values of the interactions.

Our motivation for this study was the well known fact that the chemical potential of the amphiphiles h, for fixed values of the coupling interactions, may change the nature of phase transitions in fundamental way, inducing the appearance of multicritical points. This model of the micelles has been examined, at low temperatures [16], using the Pirogov–Sinai theory of first-order phase transitions.

The layout of this paper is as follows. In section 2, we will express the lattice-gas model of the micelles in terms of Ising spin variables. In section 3, we will introduce the ground states of the model. In section 4, we will establish the free energy expression and the mean-field equations of the system considered. In section 5, we will give a description of the phase diagrams in the presence of the chemical potential of the amphiphiles (h) and the attraction interaction intermicellar parameter (J). Finally in section 6 we present our conclusions.

2. The model of the system

The Hamiltonian of the proposed model is a sum of three terms:

$$H = H_k + H_J + H_h$$

where H_k is effective at the intramicellar length scale, representing many-body interactions responsible for self-association and controlling the size and shape distribution of aggregates, and H_J describes an effective short-range coupling between the aggregates at a larger intermicellar length scale. Finally, H_h represents the usual chemical potential for controlling the concentration of amphiphiles (micelles) in the grand canonical formulation.

We assign negative energies $-K_0$ and $-K_1$, respectively, for the formation of a spherical micelle and a rodlike micelle. For an end-cap, the average $-(K_0 + K_1)/2$ is chosen.

To write H explicitly, it is convenient to use the lattice-gas variables

$$t_{i,j} = (1 + \sigma_{i,j})/2 \qquad S_{i,j} = (1 - \sigma_{i,j})/2.$$

For further convenience, we define the bilinear products

$$u_{\underline{i},j} = t_{i-1,j}t_{i+1,j}$$
$$v_{\underline{i},j} = S_{i-1,j}S_{i+1,j}$$
$$w_{\underline{i},j} = t_{i-1,j}S_{i+1,j} + S_{i-1,j}t_{i+1,j}$$

and similar ones with $i \leftrightarrow j$. In terms of these operators, H is

$$H = -K_0 \sum t\, v_{\underline{i}} v_{\underline{j}} - \tfrac{1}{2}(K_0 + K_1) \sum t\,(w_{\underline{i}} v_{\underline{j}} + v_{\underline{i}} w_{\underline{j}}) - K_1 \sum t\,(u_{\underline{i}} v_{\underline{j}} + v_{\underline{i}} u_{\underline{j}})$$
$$-J \sum S(u_{\underline{i}} + u_{\underline{j}}) - h \sum (t - s) \tag{1}$$

where we have suppressed all except the underlined indices and the summations are over all site indices [15].

The Hamiltonian H is transformed in terms of Ising variables, to the form

$$-H = J_1 \sum_{(1)} \sigma_i + J_2 \sum_{(2)} \sigma_i\sigma_j + J_3 \sum_{(3)} \sigma_i\sigma_j + J_4 \sum_{(4)} \sigma_i\sigma_j + J_5 \sum_{(5)} \sigma_i\sigma_j\sigma_k + J_6 \sum_{(6)} \sigma_i\sigma_j\sigma_k$$
$$+J_7 \sum_{(7)} \sigma_i\sigma_j\sigma_k + J_8 \sum_{(8)} \sigma_i\sigma_j\sigma_k\sigma_l + J_{(9)} \sum_{(9)} \sigma_i\sigma_j\sigma_k\sigma_l + J_{10} \sum_{(10)} \sigma_i\sigma_j\sigma_k\sigma_l\sigma_m. \tag{2}$$

The sum runs over all the spins in different sites, bonds and loops on the following cell:

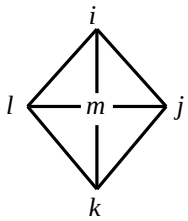

For example, the index (2), (5) and (8) indicates the sum over the following bonds (nearest-neighbour pairs) and loops respectively:

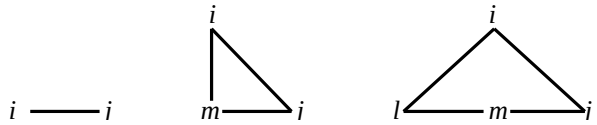

and $J_1 = (-5K_0 + 8J + 32h)/32$, $J_2 = -(4K_0 + 2K_1 + 8J)/32$, $J_3 = (2K_0 - 4K_1)/32$, $J_4 = (K_0{+}2K_1{+}4J)/32$, $J_5 = (K_0{+}2K_1{-}4J)/32$, $J_6 = (K_0{-}2K_1)/32$, $J_7 = J_8 = K_1/32$, $J_9 = J_{10} = -K_0/32$, where K_0, K_1 and J are positive. We note that the model describing the physical situation corresponds to positive values of J.

3. Ground states of the model

In order to discuss the phase diagrams of this model, it is useful to introduce the ground states of the system [16] which are defined as follows. We denote by G_1 the water ground

state (g.s.), G_2 the spherical micelles (g.s.), G_3 the rarefied spherical micelles (g.s.), G_4 the infinite rodlike micelles (g.s.), G_5 the reversed micelles (g.s.) and G_6 the amphiphile (g.s.) (see figure 1(a)).

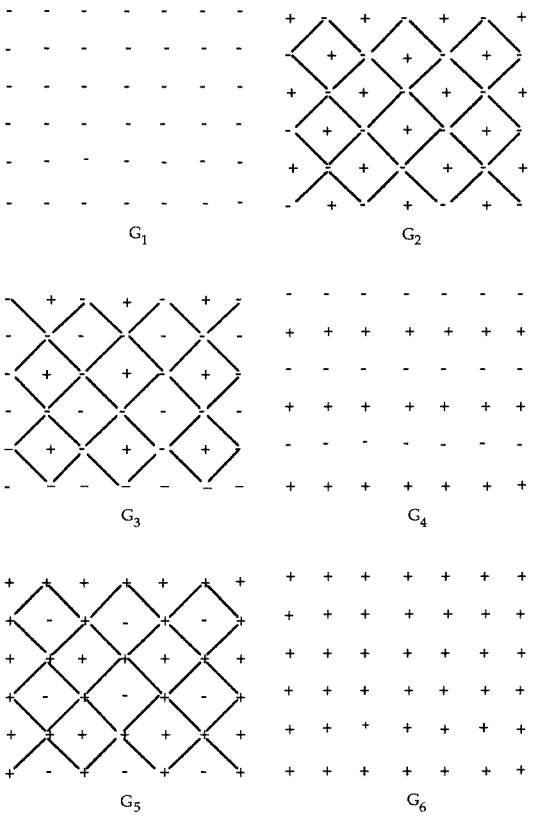

(a)

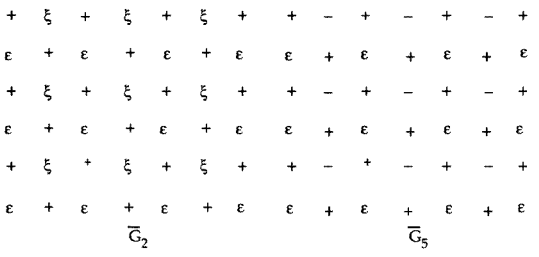

(b)

Figure 1. (a) Ground states: G_1, the water ground state (g.s.); G_2, the spherical micelles (g.s.); G_3, the rarefied spherical micelles (g.s.); G_4, the infinite rodlike micelles (g.s.); G_5, the reversed micelles (g.s.) and G_6, the amphiphile (g.s.). (b) The configurations with residual entropy of $\overline{G_5}$: the spins ε may take indifferently the value $+1$ or -1. (b) The configurations with residual entropy of $\overline{G_2}$ are governed by the following constraints. If $\xi = -1$, then the next-nearest neighbours (NNNs) (ε) of the spin ξ can take indifferently the value $+1$ or -1. If $\xi = +1$, all the NNNs of the spin ξ must take the value -1. (From [16])

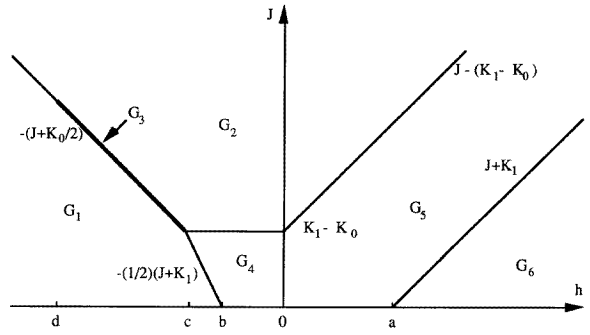

(a)

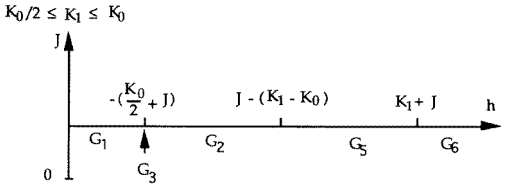

(b)

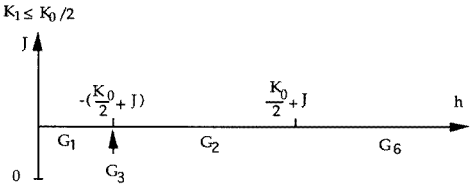

(c)

Figure 2. (a) The phase diagram at zero temperature in the space of the parameters J and h with $K_1 > K_0$. The points a, b, c and d correspond to K_1, $-K_1/2$, $-\frac{1}{2}(2K_1 - K_0)$ and $-\frac{1}{2}(4K_1 - 3K_0)$, respectively. (b) The zero-temperature phase diagram for the case where $K_0/2 \leqslant K_1 \leqslant K_0$. (c) The zero-temperature phase diagram for the case where $K_1 \leqslant K_0/2$.

The phase diagram at zero temperature of the system is given in the plan (J, h) for all values of the parameters, K_0, K_1, such that $K_1 > K_0$ (see figure 2(a)). For the case $K_1 < K_0$ we established the zero-temperature phase diagram as in figure 2(b) [16].

To characterize the different ground states, in the mean-field approximation, we introduce the parameters m_i $(i = 1, \ldots, 4)$ corresponding to four magnetizations on the four sublattices. Hence, for example, the rarefied spherical micelle ground state can be specified by $(m_1 = -1, m_2 = -1, m_3 = -1, m_4 = +1)$.

4. Mean-field equations

In the mean-field approximation the free energy F of the micellar binary solutions may be expressed as a function of the inverse temperature β, the variational parameters h_i $(i = 1, \ldots, 4)$, the magnetizations m_i $(i = 1, \ldots, 4)$ and J_i $(i = 1, \ldots, 10)$, which have

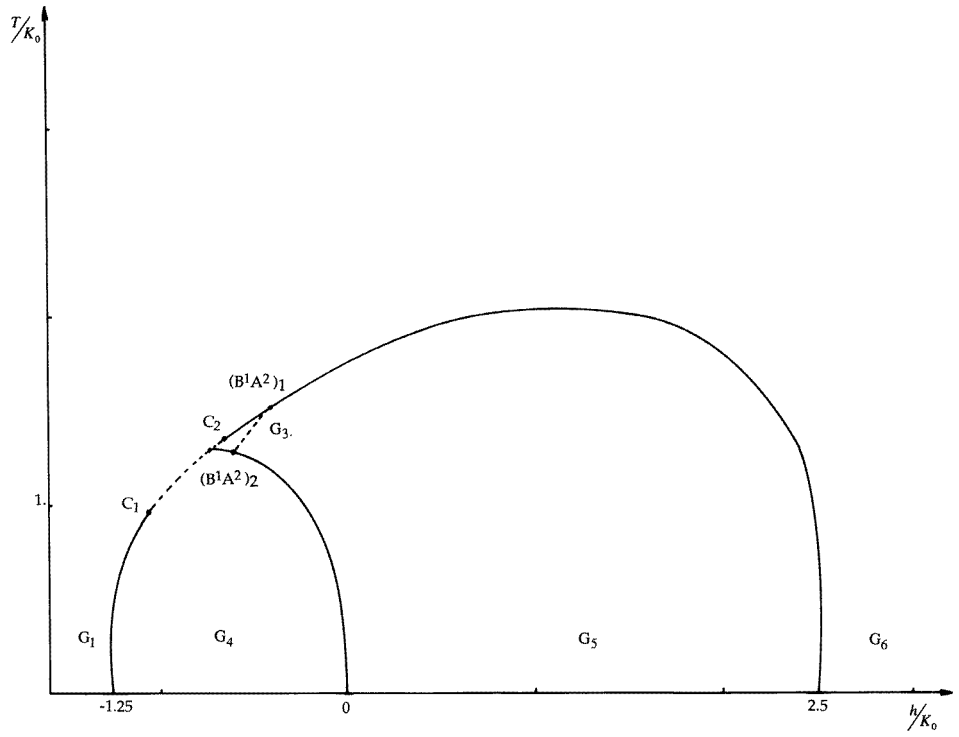

Figure 3. The phase diagram of the model for $K_1 \geqslant K_0$ and $0 \leqslant J \leqslant K_1 - K_0$ on the T–h plane (we choose, for example, $K_1/K_0 = 2$ and $J/K_0 = 0.5$). G_1, G_3, G_4, G_5 and G_6 are different pure phases. The solid lines are first-order transitions and the dashed lines are second-order transitions. There are two tricritical points C_1 and C_2 and two critical end-points $(B^1A^2)_1$ and $(B^1A^2)_2$.

been mentioned previously:

$$\begin{aligned} F = -\frac{1}{4\beta}\sum_{i=1}^{4}\log(2\cosh(\beta h_i)) + \frac{1}{4}\sum_{i=1}^{4}(h_i - J_1)m_i - (J_2/2)(m_1+m_4)(m_2+m_3) \\ -J_3(m_1m_4 + m_2m_3) - (J_4/2)(m_1^2 + m_2^2 + m_3^2 + m_4^2) \\ -(J_5/4)((m_1+m_4)(m_2^2+m_3^2) + (m_2+m_3)(m_1^2+m_4^2)) \\ -J_6(m_1m_2(m_3+m_4) + m_3m_4(m_1+m_2)) \\ -J_7(m_1m_4(m_1+m_4) + m_2m_3(m_2+m_3)) \\ -(J_8/2)(m_1m_4 + m_2m_3)(m_1+m_4)(m_2+m_3) - (J_9/2)(m_1^2m_4^2 + m_2^2m_3^2) \\ -J_{10}(m_2^2m_3^2(m_1+m_4) + m_1^2m_4^2(m_2+m_3)) \end{aligned} \tag{3}$$

where the function m_i $(i = 1, \ldots, 4)$, that is the average magnetization per spin, is given as follows:

$$m_i = \tanh(\beta h_i). \tag{4}$$

The mean-field equations in this situation are obtained by minimizing the expression of free energy F with respect to the variational parameters h_i $(i = 1, \ldots, 4)$ combined with the last expression for the magnetization. Then the first equation of this system corresponding

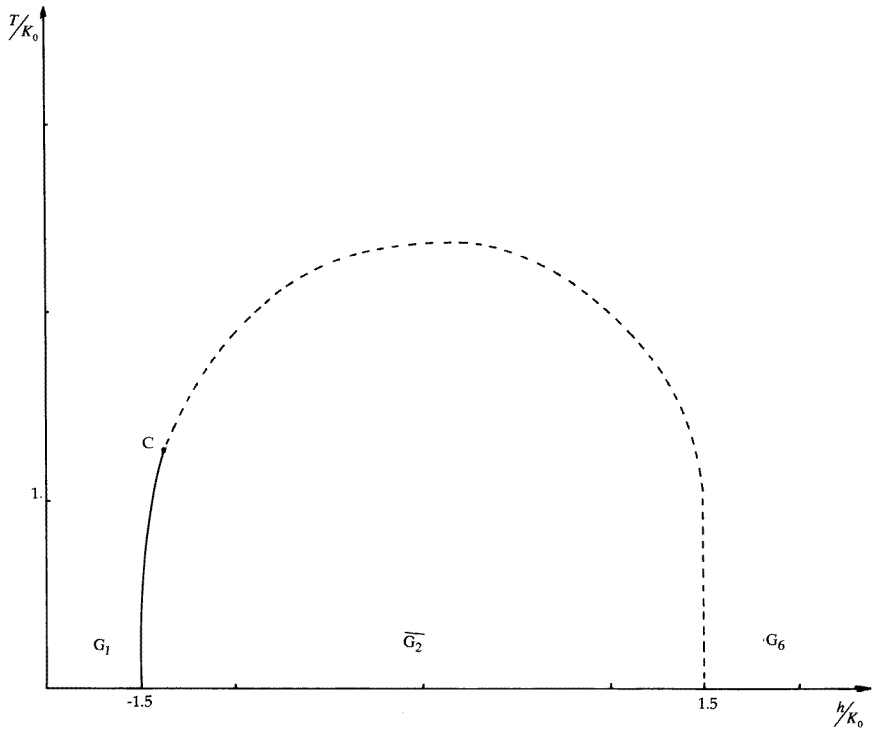

Figure 4. The phase diagram of the model for $K_1 \leqslant K_0/2$ and $J > 0$ on the T–h plane (we choose, for example, $K_1/K_0 = 0.25$ and $J/K_0 = 1$). G_1, $\overline{G_2}$ and G_6 are different pure phases. The solid lines are first-order transitions and the dashed lines are second-order transitions. The tricritical point C occurs.

to m_1 is

$$\begin{aligned} m_1 = \tanh\{\beta(J_1 &+ 2J_2(m_2+m_3) + 4J_3m_4 + 4J_4m_1 + J_5(2m_1(m_2+m_3) + (m_2^2+m_3^2)) \\ &+4J_6(m_3m_4 + m_2(m_3+m_4)) + 4J_7(m_4^2 + 2m_1m_4) \\ &+2J_8(m_2+m_3)(2m_1m_4 + m_2m_3 + m_4^2) + 4J_9m_1m_4^2 \\ &+J_{10}(m_2^2m_3^2 + 2m_1m_4^2(m_2+m_3)))\}. \end{aligned} \tag{5}$$

In order to find the three other mean-field equations corresponding to m_2, m_3 and m_4 we must exchange, respectively, $(m_1 \leftrightarrow m_2, m_3 \leftrightarrow m_4)$, $(m_1 \leftrightarrow m_3, m_2 \leftrightarrow m_4)$ and $(m_1 \leftrightarrow m_4, m_2 \leftrightarrow m_3)$.

The physically relevant solution must be found which gives the lowest value for mean-field free energy.

5. Results

The mean-field theory (MFT) should provide an adequate description of the system considered in this work. On the one hand the mean-field equations for a lattice gas model for micellar binary solutions give different regions of the phase diagrams where the phase transition lines and the multicritical points, especially critical and tricritical points, are indicated. On the other hand the analysis is restricted to the mean-field

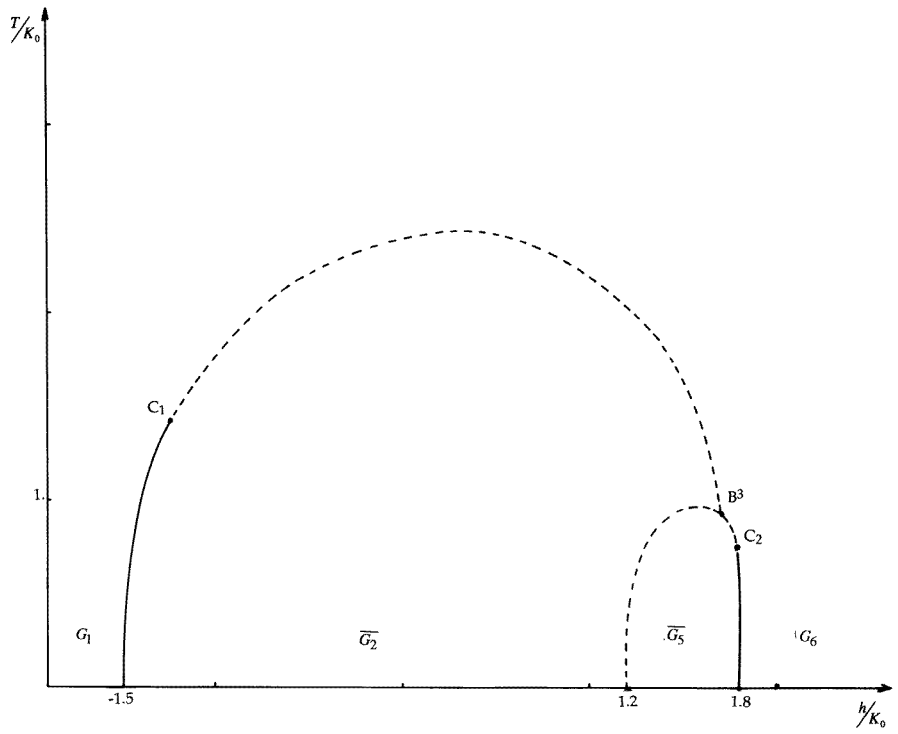

Figure 5. The phase diagram of the model for $K_0/2 \leqslant K_1 \leqslant K_0$ and $J > 0$ (we choose, for example, $K_1/K_0 = 0.8$ and $J/K_0 = 1$) on the T–h plane. G_1, $\overline{G_2}$, $\overline{G_5}$ and G_6 are different pure phases. The solid lines are first-order transitions and the dashed lines are second-order transitions. There are two tricritical points C_1 and C_2 and a multicritical point B^3.

approximation exhibiting the high-temperature region and low-temperature region which is studied analytically in [16].

In order to realize this, we construct T–h and T–J phase diagrams, which exhibit a variety of phases, for various values of the competing interactions. So, following Griffits [7], we define the critical end-point 'B^mA^n' as the intersection of a number 'm' of lines of second order and a number 'n' of lines of first order. The multicritical point 'B^m' is the intersection of a number m of lines of second order. The n-phase point 'A^n' is the intersection of a number 'n' of lines of first order. In particular we denote by 'C' the tricritical point which is the intersection of a line of second order and a line of first order.

5.1. The T–h phase diagrams

To study the phase diagrams in the (T, h) plane we propose a description of the phases of the system for different cases.

In the case $K_1 \geqslant K_0$ and $0 \leqslant J \leqslant K_1 - K_0$ (here we choose, for example, $K_1/K_0 = 2$ and $J/K_0 = 0.5$) the phase diagram shows the existence of the phases G_1, G_3, G_4, G_5 and G_6, the tricritical points C_1 and C_2 and the critical end-points $(B^1A^2)_1$ and $(B^1A^2)_2$ (figure 3). Hence, at low temperatures and for a negative value of the difference of the chemical potentials of the binary mixtures (amphiphiles–water), h, the rodlike micelles occur. Further, at higher temperatures, one can observe the rarefied spherical micelle phase

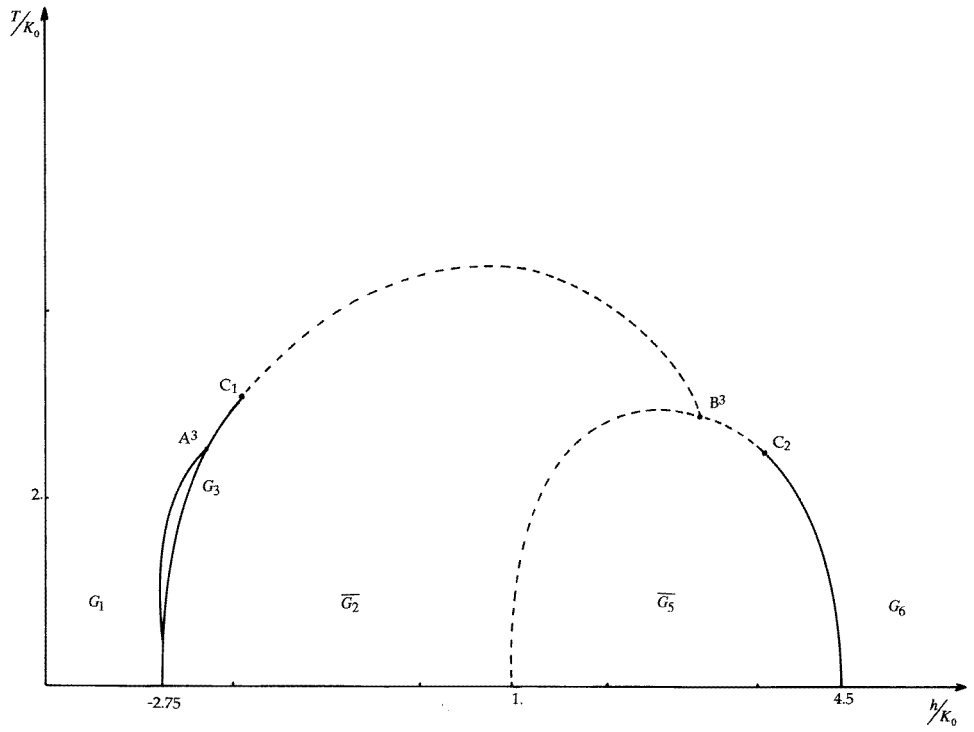

Figure 6. The phase diagram of the model for $K_1 \geqslant K_0$ and $J \geqslant K_1 - K_0$ (we choose, for example, $K_1/K_0 = 4$ and $J/K_0 = 5$) on the T–h plane. G_1, $\overline{G_2}$, G_3, $\overline{G_5}$ and G_6 are different pure phases. The solid lines are first-order transitions and the dashed lines are second-order transitions. There are two tricritical points C_1 and C_2, a multicritical point B^3 and the triple point A^3.

and the phase transition between it and the rodlike micelles is of first order. As the chemical potential (h) becomes great reversed micelles appear on the phase diagram. In comparison with the analytical investigation discussed in [16], we would like to point out that the study by means of a direct numerical analysis of the mean-field equations allows us to establish the G_3 phase (the rarefied spherical micelles) at high temperatures; these disappear at low temperatures (see figure 3).

In the case $K_1 \leqslant K_0/2$ and $J > 0$ (here we choose, for example, $K_1/K_0 = 0.25$ and $J/K_0 = 1$) the phase diagram shows the existence of the following phases: G_1, $\overline{G_2}$ and G_6, which have been defined previously except that $\overline{G_2}$ is the state with residual entropy (figure 1(b)) corresponding to G_2 as defined in [16]. Here we identified this phase by observing the four sublattice magnetizations (m_1, m_2, m_3, m_4) such that $m_1 > 0$, $m_2 < 0$, $m_3 < 0$ and $m_4 > 0$ where the sublattices corresponding to m_1 and m_4 (m_2 and m_3) are equivalent (non-equivalent). Moreover we show the existence of the tricritical point C in the phase diagram (figure 4).

In the case $K_0/2 \leqslant K_1 \leqslant K_0$ and $J > 0$ (here we choose, for example, $K_1/K_0 = 0.8$ and $J/K_0 = 1$) the phase diagram presents the phases corresponding to G_1, $\overline{G_2}$, $\overline{G_5}$ and G_6 which have been defined previously except that $\overline{G_5}$ is the state with residual entropy (figure 1(b)) corresponding to G_5 as defined in [16]. We note that this phase is characterized, in the mean-field case, by the vanishing of the magnetization in some

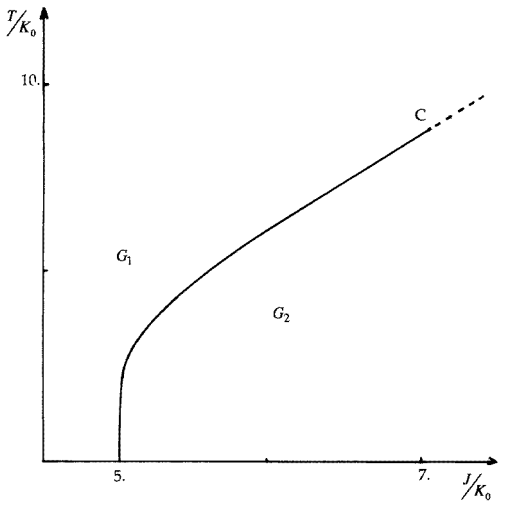

Figure 7. The phase diagram of the model for $h < -\frac{1}{2}(4K_1 - 3K_0)$ (for example, $K_1/K_0 = 2$ and $h/K_0 = -3$) on the T–J plane. G_1 and G_2 are the pure phases. The solid lines are first order transitions and the dashed lines are second order transitions. The tricritical point C occurs.

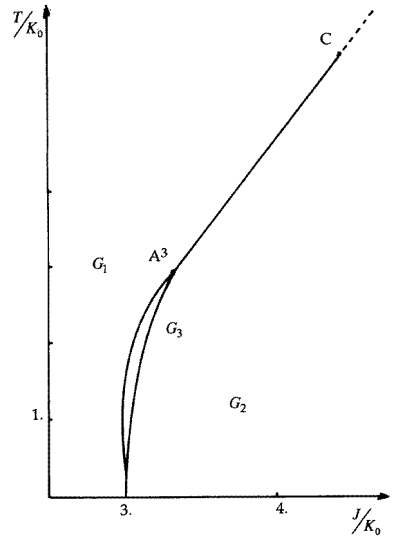

Figure 8. The phase diagram of the model for $h \in [-\frac{1}{2}(4K_1 - 3K_0), -\frac{1}{2}(2K_1 - K_0)]$ (for example, $K_1/K_0 = 2$ and $h/K_0 = -2$) on the T–J plane. G_1, G_2 and G_3 are different pure phases. The solid lines are first-order transitions and the dashed lines are second-order transitions. The triple point A^3 and the tricritical point C occur.

sublattice at $h = J - (K_1 - K_0)$ (e.g. $h/K_0 = 1.2$). For $h > J - (K_1 - K_0)$ (e.g. $h/K_0 > 1.2$) the magnetization on this sublattice increases continuously with h/K_0 from 0 to $+1$. Moreover, in this phase diagram we note the existence of two tricritical points C_1 and C_2 and a multicritical point B^3 (figure 5). For a negative value of the chemical potential (h) of the amphiphiles the phase with residual entropy corresponding to spherical micelles

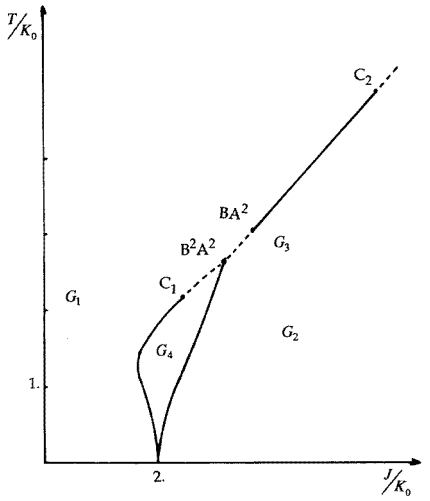

Figure 9. The phase diagram of the model for $h = -\frac{1}{2}(2K_1 - K_0)$ (for example, $K_1/K_0 = 2$ and $h/K_0 = -1.5$) on the T–J plane. G_1, G_2, G_3 and G_4 are different pure phases. The solid lines are first order transitions and the dashed lines are second order transitions. There are two critical end-points of type B^2A^2 and BA^2 and two tricritical points C_1 and C_2.

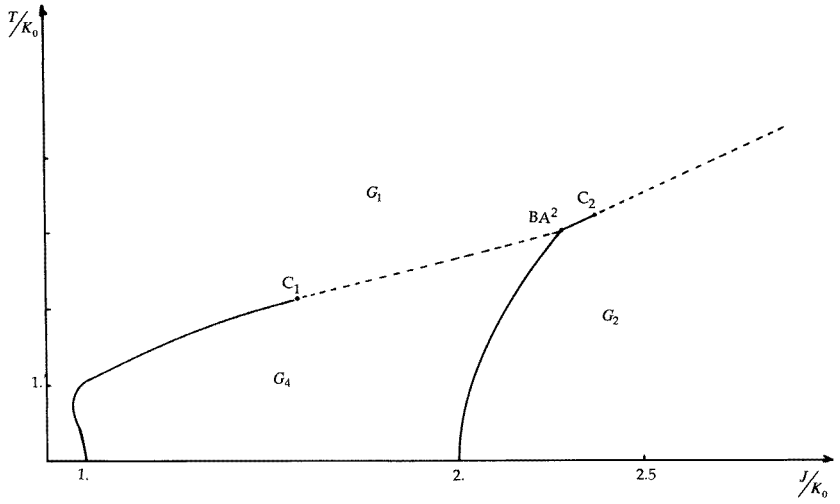

Figure 10. The phase diagram of the model for $h \in [-\frac{1}{2}(2K_1 - K_0), -K_1/2]$ (for example, $K_1/K_0 = 2$ and $h/K_0 = -1.25$) on the T–J plane. G_1, G_2 and G_4 are different pure phases. The solid lines are first-order transitions and the dashed lines are second order transitions. The critical end-point BA^2 and the tricritical points C_1 and C_2 occur.

exists but as h becomes great the phase with residual entropy corresponding to reversed micelles occurs and the transition between them is of second order.

In the case $K_1 \geqslant K_0$, $J \geqslant K_1 - K_0$ (here we choose, for example, $K_1/K_0 = 4$ and $J/K_0 = 5$) the phase diagram presents the phases corresponding to G_1, $\overline{G_2}$, G_3, $\overline{G_5}$ and G_6, two tricritical points C_1 and C_2, a multicritical point B^3 and the triple point A^3 (figure 6). In

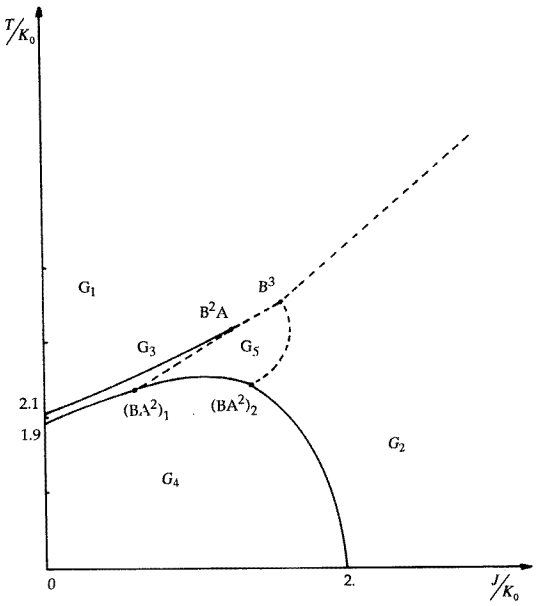

Figure 11. The phase diagram of the model for $h \in [-K_1/2, 0]$ (for example, $K_1/K_0 = 2$ and $h/K_0 = -0.5$) on the T–J plane. G_2 and G_4 are the pure phases. The solid lines are first-order transitions and the dashed lines are second order transitions. The critical end-points $(BA^2)_1$, $(BA^2)_2$ and B^2A and the multicritical point B^3 occur.

this phase diagram, we point out that the rarefied spherical micelles phase can be observed at low temperature and for a negative values of the chemical potential (h) of the amphiphiles.

5.2. The T–J phase diagrams

The phase diagrams in the (T, J) plane are given here for different cases.

In the case $h < -\frac{1}{2}(4K_1 - 3K_0)$ (here we choose, for example, $K_1/K_0 = 2$ and $h/K_0 = -3$) the phase diagram presents the phases corresponding to G_1 and G_2 and the tricritical point C (figure 7).

In the case $h \in [-\frac{1}{2}(4K_1 - 3K_0) - \frac{1}{2}(2K_1 - K_0)]$ (here we choose, for example, $K_1/K_0 = 2$ and $h/K_0 = -2$) the phase diagram presents the phases corresponding to G_1, G_2 and G_3, the triple point A^3 and the tricritical point C (figure 8). We note here that, by increasing the intermicellar attraction parameter (J), one can obtain a first-order transition from the rarefied spherical micelle phase to the spherical micelle phase.

In the case $h = -\frac{1}{2}(2K_1 - K_0)$ (here we choose, for example, $K_1/K_0 = 2$ and $h/K_0 = -1.5$) the phase diagram presents the phases corresponding to G_1, G_2, G_3 and G_4, the critical end-points of type B^2A^2 and BA^2 and the tricritical points C_1 and C_2 (figure 9). We find that this phase diagram that for certain values of J and at low temperatures rodlike micelles occur, and for higher temperatures one can reach the rarefied spherical micelle phase. In the case $h \in [-\frac{1}{2}(2K_1 - K_0), -K_1/2]$ (here we choose, for example, $K_1/K_0 = 2$ and $h/K_0 = -1.25$) the phase diagram presents the phases corresponding to G_1, G_2 and G_4, the critical end-point BA^2 and the tricritical points C_1 and C_2 (figure 10). In this phase diagram we note that there exists a first-order transition between the phases corresponding to the rodlike micelles and the spherical micelles.

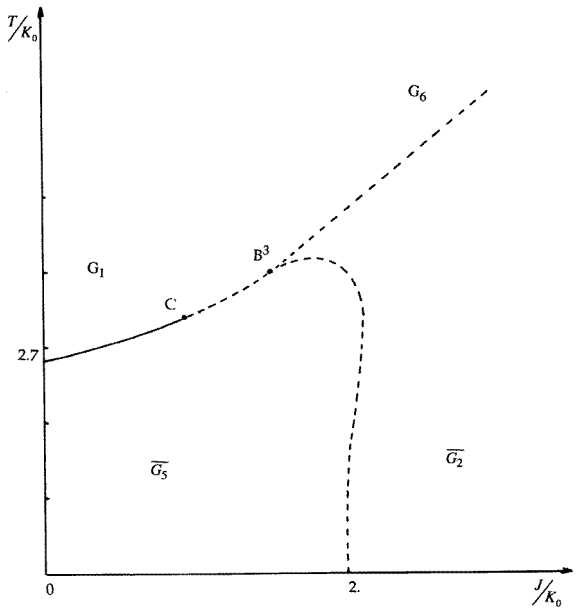

Figure 12. The phase diagram of the model for $h = 0$ (for example, $K_1/K_0 = 2$ and $h/K_0 = 0$) on the T–J plane. $\overline{G_2}$ and $\overline{G_5}$ are the pure phases. The solid lines are first-order transitions and the dashed lines are second-order transitions. The tricritical point C and the multicritical point B^3 occurs.

In the case $h \in [-K_1/2, 0]$ (here we choose, for example, $K_1/K_0 = 2$ and $h/K_0 = -0.5$) the phase diagram presents the phases corresponding to G_1, G_2, G_3, G_4 and G_5, the critical end-points $(BA^2)_1$, $(BA^2)_2$ and B^2A and the multicritical point B^3 (figure 11). At low temperatures we find that there exists a first-order transition between the rodlike micelle phase and the spherical micelle phase as we vary the attraction intermicellar parameter J, but for high temperatures we can observe a second-order transition between the rarefied spherical micelle phase and the reversed micelle phase and another between the latter and the spherical micelle phase.

In the case $h = 0$ (here we choose, for example, $K_1/K_0 = 2$ and $h/K_0 = 0$) the phase diagram presents the phases corresponding to G_1, $\overline{G_2}$ and $\overline{G_5}$, the tricritical point C, and the multicritical point B^3 (figure 12). We point out that although there is a coexistence of two ground states (G_4, G_5), at zero temperature for $0 < J < K_1 - K_0$, only one phase appears at non-zero temperatures.

In the case $h \in [0, K_1]$ (here we choose, for example, $K_1/K_0 = 2$ and $h/K_0 = 1$) the phase diagram shows the existence of the phases $\overline{G_2}$, $\overline{G_5}$ and G_6 and the critical end-point BA^2 (figure 13).

In the case $h > K_1$ (here we choose, for example, $K_1/K_0 = 2$ and $h/K_0 = 3$) the phase diagram shows the existence of the phases $\overline{G_2}$, $\overline{G_5}$, and G_6, and the critical end-point BA^2 (figure 14).

On the phase diagrams in figures 13 and 14 we note only the existence of the first-order transition between the phases with residual entropy corresponding to reversed micelles and spherical micelles as we vary the attraction intermicellar parameter J.

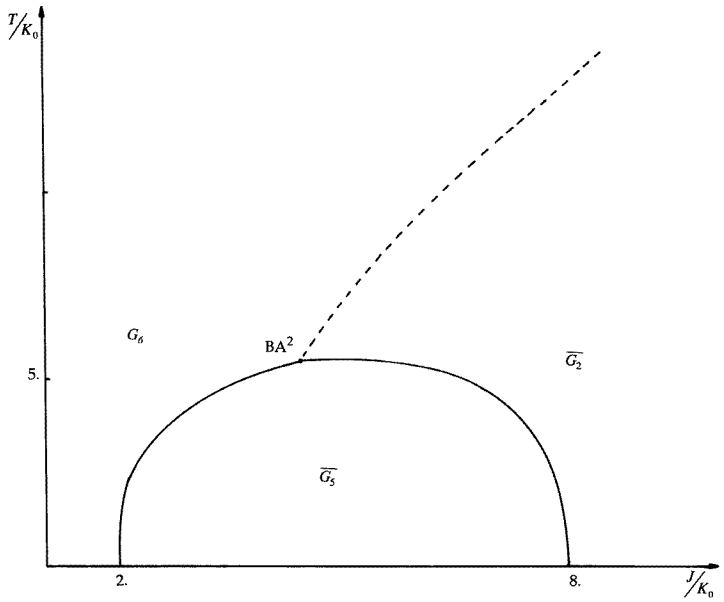

Figure 13. The phase diagram of the model for $h \in [0, K_1]$ (for example, $K_1/K_0 = 2$ and $h/K_0 = 1$) on the T–J plane. $\overline{G_2}$, $\overline{G_5}$ and G_6 are the pure phases. The solid lines are first-order transitions and the dashed lines are second-order transitions. The critical end-point BA^2 occurs.

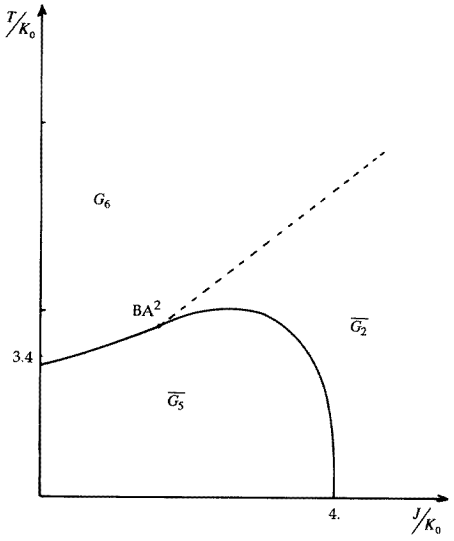

Figure 14. The phase diagram of the model for $h > K_1$ (for example, $K_1/K_0 = 2$ and $h/K_0 = 3$) on the T–J plane. $\overline{G_2}$, $\overline{G_5}$, and G_6 are the pure phases. The critical end-point BA^2 occurs.

6. Conclusions

We have presented, in this paper, some new theoretical and numerical results concerning the phase diagrams of the micellar binary solutions. This allows us to check that the conjecture

proposed by Shnidman and Zia about the behaviour of the phase diagrams is correct, so we point out that this work has completed the earlier study of [16] by giving the complete description of the phase diagrams and the nature of their transition lines. Therefore, the study by means of a direct numerical analysis of the mean-field equations allows us to establish the G_3 phase (the rarefied spherical micelles) at high temperatures; these disappear at low temperatures (see figures 3, 9 and 11).

References

[1] Dawson K A and Kurtovic Z 1990 *J. Chem. Phys.* **92** 5473
[2] Halley J W and Kolan A J 1988 *J. Chem. Phys.* **88** 3313
[3] Matsen M W and Sullivan D E 1990 *Phys. Rev.* A **41** 2021
[4] Gompper G and Schick M 1989 *Chem. Phys. Lett.* **163** 475
[5] Gompper G and Schick M 1994 *Self-Assembling Amphiphilic Systems in Phase Transitions and Critical Phenomena* vol 16, ed C Domb and J L Lebowitz (London: Academic)
[6] Gelbart W M, Roux D and Ben-Shaul A (ed) 1994 *Micelles, Membranes, Microemulsions and Monolayers* (Berlin: Springer)
[7] Degiorgio V and Corti M (ed) 1985 *Physics of Amphiphiles: Micelles, Vesicles and Microemulsions* (Amsterdam: North-Holland)
[8] Tiddy G J T 1980 *Phys. Rep.* **57** 1
[9] Gompper G and Zschocke S 1991 *Europhys. Lett.* **16** 731
[10] Seddon J M 1990 *Biochim. Biophys. Acta* **1031** 1
[11] Hoffmann H 1990 *Adv. Colloid Interface Sci.* **32** 123
[12] Strey R, Schomäcker R, Roux D, Frederic F and Olsson U 1990 *J. Chem. Soc. Faraday Trans.* **86** 2253
[13] Degiorgio V, Corti M and Cantu L 1988 *Chem. Phys. Lett.* **151** 349
[14] Israelachvili J N, Mitchell D J and Ninham B W 1976 *J. Chem. Soc. Faraday Trans.* **72** 1525
[15] Shnidman Y and Zia R K P 1988 *J. Stat. Phys.* **50** 839
[16] Benyoussef A, Laanait L and Moussa N 1993 *Phys. Rev.* B **48** 16 310